Optica Applicata, Vol. LV, No. 3, 2025
DOI: 10.37190/oa/204501

Focusing field transverse energy flow simulation of azimuthally polarized Lorentz–Gaussian beam modulated by power order space-variant phase

CHUNDI ZHENG[1], ZIJIE ZHOU[1,2], GUOJIN FENG[1], JINSONG LI[2,*]

[1] National Institute of Metrology, Beijing 10029, P.R. China

[2] China Jiliang University, College of Optics and Electronic, Hangzhou 310018, P.R. China

[*] Corresponding author: lijinsong@cjlu.edu.cn,

On the basis of the vector diffraction theory, this article investigates the transverse energy flow distributions of azimuthally polarized Lorentz–Gaussian beams modulated by power order space-variant phase modulation. The findings of the study show that the distribution of transverse energy flow is significantly affected by variations in the power order of the space-variant phase n. We obtained circular distribution, two zone distribution, bullet-shaped distribution, and reverse Z-distribution. Furthermore, it can be observed that the variation of phase change parameter C will affect the transverse energy flow distributions, while the variation of topological charge m will lead to the diffusion of energy. These phenomena may assist in capturing specific particles.

Keywords: Lorentz–Gaussian beam, vector diffraction theory, transverse energy flow.

1. Introduction

The Lorentz beam, which was first presented by EL GAWHARY *et al*. [1-3] has garnered a lot of interest from scientists lately [4-10]. MIAO successfully achieved ideal beam shaping by adjusting the beam parameters of diagonally polarized Lorentz–Gaussian beams. In addition, MIAO also generated the required beam with specific parameters through holographic methods [11]. SHAMSODINI *et al*. investigated how the focusing properties of four-petal Lorentz–Gaussian beams were affected by beam parameters and severely nonlinear nonlocal medium factors [12]. SUN *et al*. investigated how the concentrated optical field distribution of Airy–Lorentz–Gaussian beams was affected by triangle phase and beam characteristics [13]. In a paraxial optical ABCD system, EBRAHIM *et al*. investigated how various beam parameters affected the transmission properties of circular Lorentz–Bessel–Gaussian beams [14].

Azimuthally polarized beams belong to a type of cylindrical vector beam and have always been a focus of research for many researchers [15-19]. CHI *et al*. compared

the focusing characteristics of azimuthally polarized beams and radially polarized beams, and ultimately obtained ultra long super-resolution optical needles using azimuthally polarized beams and ideal binary phase elements [20]. After azimuthally polarized Laguerre–Gaussian vortex beams passed through various optical elements, ALKELLY *et al*. investigated the focusing properties of these beams. By adjusting certain parameters, these distinctive focal forms can be produced [21]. In a 4π focusing system, YANG *et al*. investigated the focusing properties of azimuthally polarized Laguerre –Gaussian beams and, by varying the parameters, were able to get three focusing modes [22]. At the same time, the energy flow distribution of light beams has also received a lot of attention from researchers [23-26]. KHONINA *et al*. attempted to generate reverse energy flow using cylindrical vector beams [27]. By modifying the pertinent radially polarized vortex beam parameters and meeting a certain relationship, CHEN *et al*. can achieve negative energy flow in the focal region [28]. KOTLYAR *et al*. studied the influence of optical vortices on the energy flow of cylindrical vector beams, and three types of energy flows can be achieved by changing the conditions [29]. The transverse energy flow distributions of azimuthally polarized Lorentz–Gaussian beams modulated by power order space-variant phase modulation have not yet been investigated.

Precise control of transverse energy flow is of great significance for applications like optical trapping and optical communication. Specifically, by modulating spatial parameters such as the polarization distribution and topological charge of vector vortex beams, transverse energy flow can be achieved in a tightly-focused system, thus promoting the development of the field of optical field control. This paper will discuss the transverse energy flow distributions in the focusing field of an azimuthally polarized Lorentz–Gaussian beam modulated by power order space-variant phase under various conditions, such as altering the topological charge, power order of the space -variant phase, and phase change parameter.

2. Theory

A high numerical aperture objective lens focuses an azimuthally polarized Lorentz –Gaussian beam that has been filtered by a phase plate to create a tightly focused light field, as shown as Fig. 1.

The Lorentz–Gaussian incident beam in the focusing optical system is expressed as follows:

$$E(\theta, \varphi) = \exp\left(-\frac{\cos^2\varphi \sin^2\theta}{\mathrm{NA}^2 w_x^2}\right) \frac{1}{1 + \dfrac{\sin^2\varphi \sin^2\theta}{\mathrm{NA}^2 \gamma_y^2}} \exp(im\varphi) \tag{1}$$

where φ is the azimuthal angle, θ is the convergence angle, and $\theta \in [0, \arcsin(\mathrm{NA})]$. The numerical aperture of this focusing mechanism is denoted by NA and m denotes

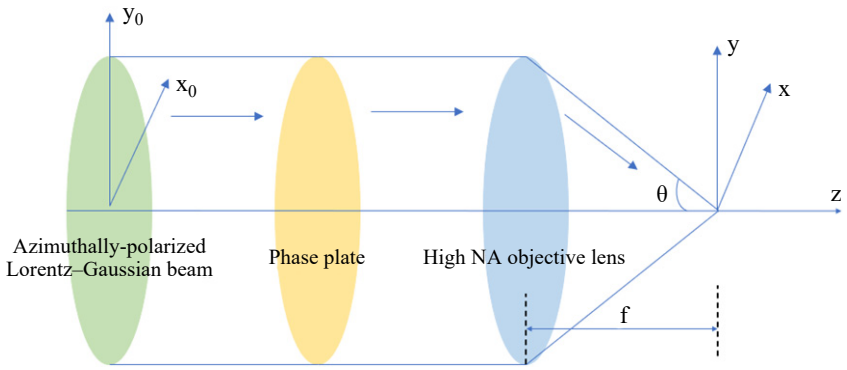

Fig. 1. System structure diagram.

the topological charge of the vortex. w_x is relative Gaussian parameter and γ_y is relative Lorentzian parameter.

The phase on the phase plate can be represented as

$$\Delta = 2\pi C\left(\frac{\sin\theta\cos\varphi}{\sin\theta_{\max}}\right)^n \tag{2}$$

where C is a phase change parameter, n is the power order of the space-variant phase, and $\theta_{\max}$ is the maximum convergence angle. It is worth mentioning that $r = f\sin\theta$ and $r_0 = f\sin\theta_{\max}$, where f is the focal length, so the ratio of $\sin\theta$ to $\sin\theta_{\max}$ in the phase can be evolved from r/r_0, and this makes the phase related to both radial and angular components; thus, the power order phase gets a space-variant distribution.

The azimuthally polarized Lorentz–Gaussian beam modulated by power order space-variant phase in the focusing optical system can be expressed as follows using Eqs. (1) and (2):

$$E(\theta,\varphi) = \exp\left(-\frac{\cos^2\varphi\,\sin^2\theta}{\mathrm{NA}^2 w_x^2}\right)\frac{1}{1+\dfrac{\sin^2\varphi\,\sin^2\theta}{\mathrm{NA}^2\gamma_y^2}}\exp(im\varphi)\exp(i\Delta) \tag{3}$$

According to the vectorial diffraction theory [30,31], the intensity of the electric field in the focal region can be represented as

$$E(\rho,\psi,z) = \frac{-ikf}{2\pi}\iint_{\Omega}\left\{\begin{array}{l} E(\theta,\varphi)\left[(-\sin\varphi)x + (\cos\varphi)y + 0\cdot z\right]\sin\theta\sqrt{\cos\theta} \\ \times\exp\left[-ik\rho\sin\theta\cos(\varphi-\psi)\right]\exp(-ikz\cos\theta)\end{array}\right\}\mathrm{d}\theta\,\mathrm{d}\varphi \tag{4}$$

Substituting Eq. (3) into Eq. (4), the electric field in the direction of x is

$$E_x(\rho, \psi, z) = \frac{-ikf}{2\pi} \int_0^{2\pi} \int_0^{\theta_{\max}} \left\{ \begin{array}{l} \sqrt{\cos\theta}\, \exp\left(-\dfrac{\cos^2\varphi \sin^2\theta}{\mathrm{NA}^2 w_x^2}\right) \dfrac{1}{1+\dfrac{\sin^2\varphi \sin^2\theta}{\mathrm{NA}^2 \gamma_y^2}} \\ \times \exp(im\varphi) \exp(i\Delta) \sin\theta(-\sin\varphi) \\ \times \exp\left[-ik\rho \sin\theta \cos(\varphi - \psi)\right] \exp(-ikz\cos\theta) \end{array} \right\} \mathrm{d}\theta\, \mathrm{d}\varphi \tag{5}$$

The electric field in the direction of y is

$$E_y(\rho, \psi, z) = \frac{-ikf}{2\pi} \int_0^{2\pi} \int_0^{\theta_{\max}} \left\{ \begin{array}{l} \sqrt{\cos\theta}\, \exp\left(-\dfrac{\cos^2\varphi \sin^2\theta}{\mathrm{NA}^2 w_x^2}\right) \dfrac{1}{1+\dfrac{\sin^2\varphi \sin^2\theta}{\mathrm{NA}^2 \gamma_y^2}} \\ \times \exp(im\varphi) \exp(i\Delta) \sin\theta\cos\varphi \\ \times \exp\left[-ik\rho \sin\theta \cos(\varphi - \psi)\right] \exp(-ikz\cos\theta) \end{array} \right\} \mathrm{d}\theta\, \mathrm{d}\varphi \tag{6}$$

The electric field in the direction of z is

$$E_z(\rho, \psi, z) = 0 \tag{7}$$

where $k = 2\pi/\lambda$ is the wavenumber, λ is the wavelength of the incident beam, and f is the focal length of the focusing objective.

The intensity of the magnetic field in the focal region can be represented as

$$\mathbf{H} = k_0 \times \mathbf{E} \tag{8}$$

where the unit vector of the wave vector is denoted as k_0 and it can be written as

$$k_0 = (-\sin\theta\cos\varphi, -\sin\theta\sin\varphi, \cos\theta) \tag{9}$$

Substituting Eq. (9) and Eq. (3) into Eq. (8), the magnetic field in the direction of x is

$$H_x(\rho, \psi, z) = \frac{-ikf}{2\pi} \int_0^{2\pi} \int_0^{\theta_{\max}} \left\{ \begin{array}{l} \sqrt{\cos\theta}\, \exp\left(-\dfrac{\cos^2\varphi \sin^2\theta}{\mathrm{NA}^2 w_x^2}\right) \dfrac{1}{1+\dfrac{\sin^2\varphi \sin^2\theta}{\mathrm{NA}^2 \gamma_y^2}} \\ \times \exp(im\varphi) \exp(i\Delta) \sin\theta(-\cos\varphi\cos\theta) \\ \times \exp\left[-ik\rho \sin\theta \cos(\varphi - \psi)\right] \exp(-ikz\cos\theta) \end{array} \right\} \mathrm{d}\theta\, \mathrm{d}\varphi \tag{10}$$

The magnetic field in the direction of y is

$$H_y(\rho, \psi, z) = \frac{-ikf}{2\pi} \int_0^{2\pi} \int_0^{\theta_{\max}} \left\{ \begin{array}{l} \sqrt{\cos\theta}\, \exp\left(-\dfrac{\cos^2\varphi \sin^2\theta}{\mathrm{NA}^2 w_x^2} \right) \dfrac{1}{1 + \dfrac{\sin^2\varphi \sin^2\theta}{\mathrm{NA}^2 \gamma_y^2}} \\ \times \exp(im\varphi) \exp(i\Delta) \sin\theta(-\sin\varphi\cos\theta) \\ \times \exp\left[-ik\rho \sin\theta \cos(\varphi - \psi) \right] \exp(-ikz\cos\theta) \end{array} \right\} \mathrm{d}\theta\, \mathrm{d}\varphi \tag{11}$$

The magnetic field in the direction of z is

$$H_z(\rho, \psi, z) = \frac{-ikf}{2\pi} \int_0^{2\pi} \int_0^{\theta_{\max}} \left\{ \begin{array}{l} \sqrt{\cos\theta}\, \exp\left(-\dfrac{\cos^2\varphi \sin^2\theta}{\mathrm{NA}^2 w_x^2} \right) \dfrac{1}{1 + \dfrac{\sin^2\varphi \sin^2\theta}{\mathrm{NA}^2 \gamma_y^2}} \\ \times \exp(im\varphi) \exp(i\Delta) \sin\theta(-\sin\theta) \\ \times \exp\left[-ik\rho \sin\theta \cos(\varphi - \psi) \right] \exp(-ikz\cos\theta) \end{array} \right\} \mathrm{d}\theta\, \mathrm{d}\varphi \tag{12}$$

The Poynting vector can be represented as [32,33]

$$S = \frac{c}{8\pi} \mathrm{Re}[E \times H^*] \tag{13}$$

3. Numerical results

The aforementioned formulas are used to simulate the distributions of the transverse energy flow on the focal plane under different values of n, m and C. In this article, the parameters are selected as follows: the numerical aperture of the focusing optical system NA = 0.95, the wavelength λ = 632.8 nm, the relative Gaussian parameter w_x = 1.2, and the relative Lorentzian parameter γ_y = 1.6.

Firstly, we set the power order variable phase to 0 and only discuss the influence of topological charges on the transverse energy flow distribution. Figure 2 shows the energy flow distribution of an azimuthally polarized Lorentz–Gaussian beam when n = 0, C = 0, and different values of m. When m = 0, the beam is not subjected to any phase modulation, and the distribution range of transverse energy flow is small and solid, as shown in Fig. 2(a). When m = 1, the distribution range of transverse energy flow becomes larger and exhibits a circular distribution, as shown in Fig. 2(b). When m = 2, the size of the hollow area increases along with the transverse energy flow ring's radius, as shown in Fig. 2(c). When m = 3, the radius of the flow ring continues to increase, as shown in Fig. 2(d). It is evident that as m increases, the transverse energy

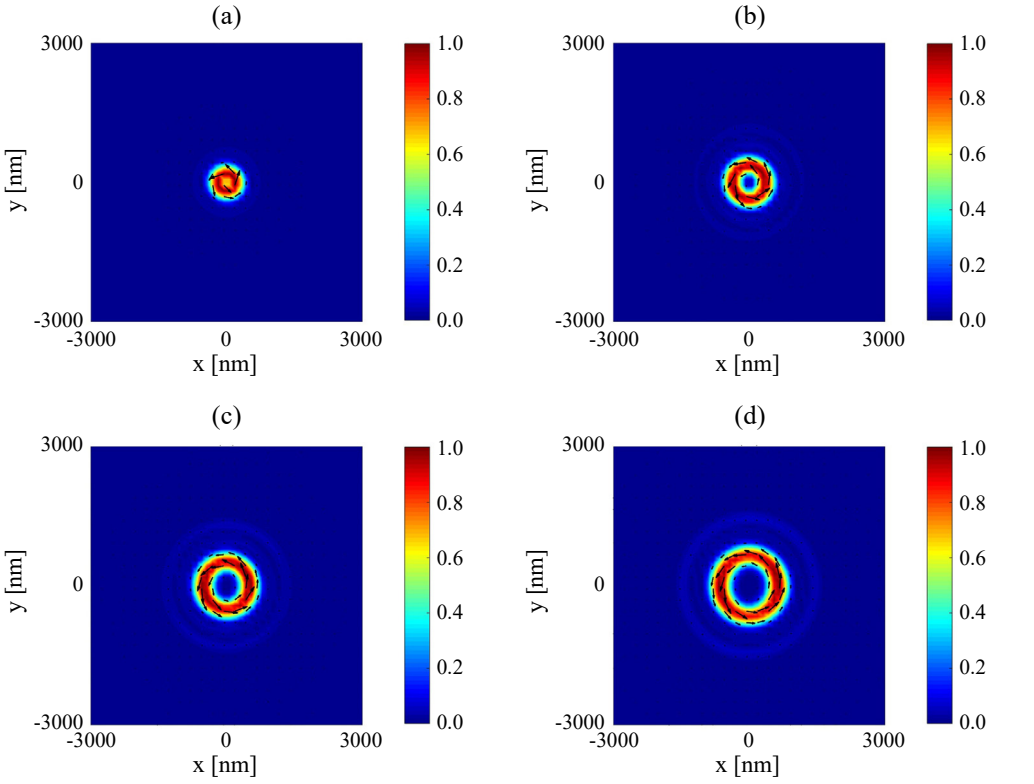

Fig. 2. Normalized transverse (S_{x+y}) energy flow distributions when $n = 0$, $C = 0$ and (a) $m = 0$, (b) $m = 1$, (c) $m = 2$, and (d) $m = 3$. The directional orientation of energy flow is represented by the black arrows.

flow ring's radius progressively grows. In Fig. 2(a)–(d), the energy flow is in a counterclockwise direction.

Figure 3 shows the transverse energy flow distributions of an azimuthally polarized Lorentz–Gaussian beam when $n = 1$, $m = 3$, and different C. When $C = 0$, the transverse energy flow exhibits a circular distribution, as shown in Fig. 3(a). When $C = -1$, the transverse energy flow ring exhibits a tendency to shift in the direction of the negative x-axis, as shown in Fig. 3(b). When $C = -2$, the transverse energy flow ring keeps moving in the negative direction of x-axis, as shown in Fig. 3(c). When comparing the transverse energy flow ring when $C = 1$ with that when $C = 0$, the transverse energy flow ring tends to shift in the positive direction of the x-axis, as shown in Fig. 3(d). When C increases from 1 to 3, the transverse energy flow ring continues to move in the positive direction of x-axis, as shown in Fig. 3(e) and (f), respectively. It can be observed that as C increases in the positive direction, the transverse energy flow ring gradually moves towards the positive x-axis direction. When C is negative, as C gradually decreases, the transverse energy flow ring gradually moves towards the negative direction of x-axis. This provides assistance in capturing particles at different locations. In Fig. 3(a)–(e), the energy flow is in a counterclockwise direction.

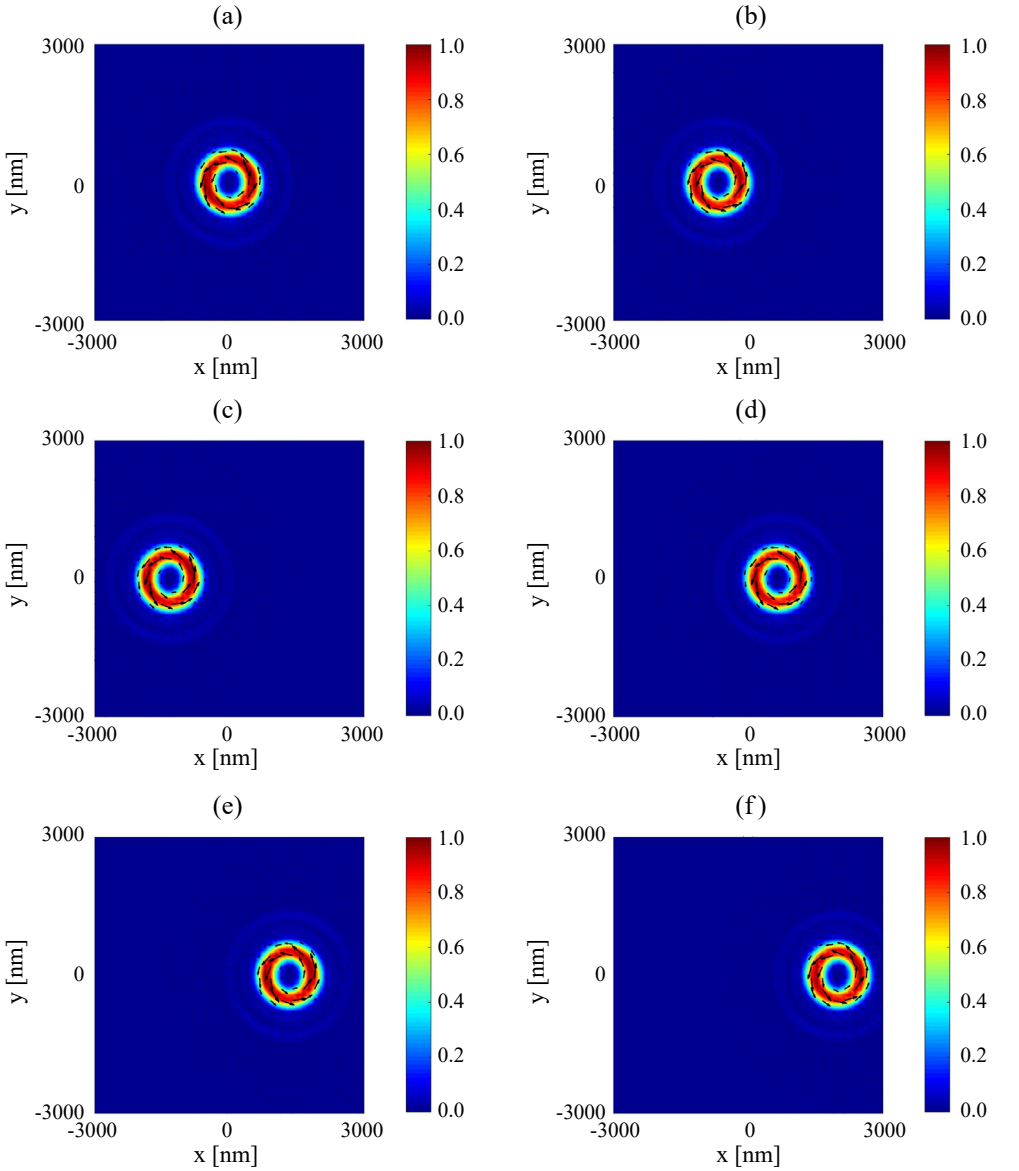

Fig. 3. Normalized transverse (S_{x+y}) energy flow distributions when $n = 1$, $m = 3$, and (a) $C = 0$, (b) $C = -1$, (c) $C = -2$, (d) $C = 1$, (e) $C = 2$, and (f) $C = 3$. The directional orientation of energy flow is represented by the black arrows.

Figure 4 shows the transverse energy flow distributions of an azimuthally polarized Lorentz–Gaussian beam when $n = 2$, $m = 3$, and different C. When $C = -1$, the transverse energy flow consists of two parts that are mutually opposed, as shown in Fig. 4(a). When $C = -2$, the energy flow distribution on the left moves in the x-axis's negative direction, whereas the energy flow distribution on the right moves in the x-axis's pos-

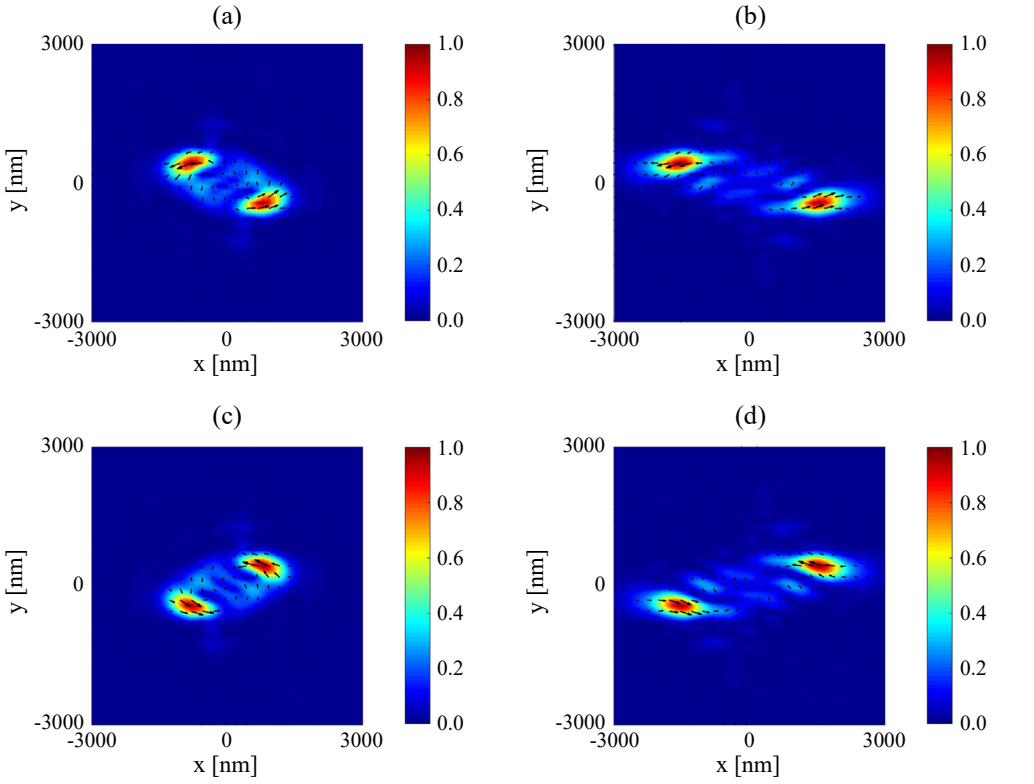

Fig. 4. Normalized transverse (S_{x+y}) energy flow distributions when $n = 2$, $m = 3$ and (a) $C = -1$, (b) $C = -2$, (c) $C = 1$, and (d) $C = 2$. The directional orientation of energy flow is represented by the black arrows.

itive direction, as shown in Fig. 4(b). By comparing the transverse energy flow distribution at $C = 1$ with that at $C = -1$, we can find that the transverse energy flow distribution in both cases is centrally symmetrical, as shown in Fig. 4(c) and Fig. 4(a), respectively. When $C = 2$, the energy flow distribution on the left moves in the negative direction of x-axis, whereas the energy flow distribution on the right moves in the positive direction of x-axis, as shown in Fig. 4(d). From the above, it can be seen that when C is a positive number, the gradual increase of C will cause the two parts of the energy flow distribution to gradually move away. When C is a negative number, the gradual decrease of C will cause the two parts of the energy flow distribution to gradually move away, and the energy flow distribution in both cases shows different directions of movement. In Fig. 4(a)–(d), the energy flow of both parts is in a counterclockwise direction.

Figure 5 shows the transverse energy flow distributions of an azimuthally polarized Lorentz–Gaussian beam when $n = 3$, $C = 3$, and different m. When $m = 1$, the trans-

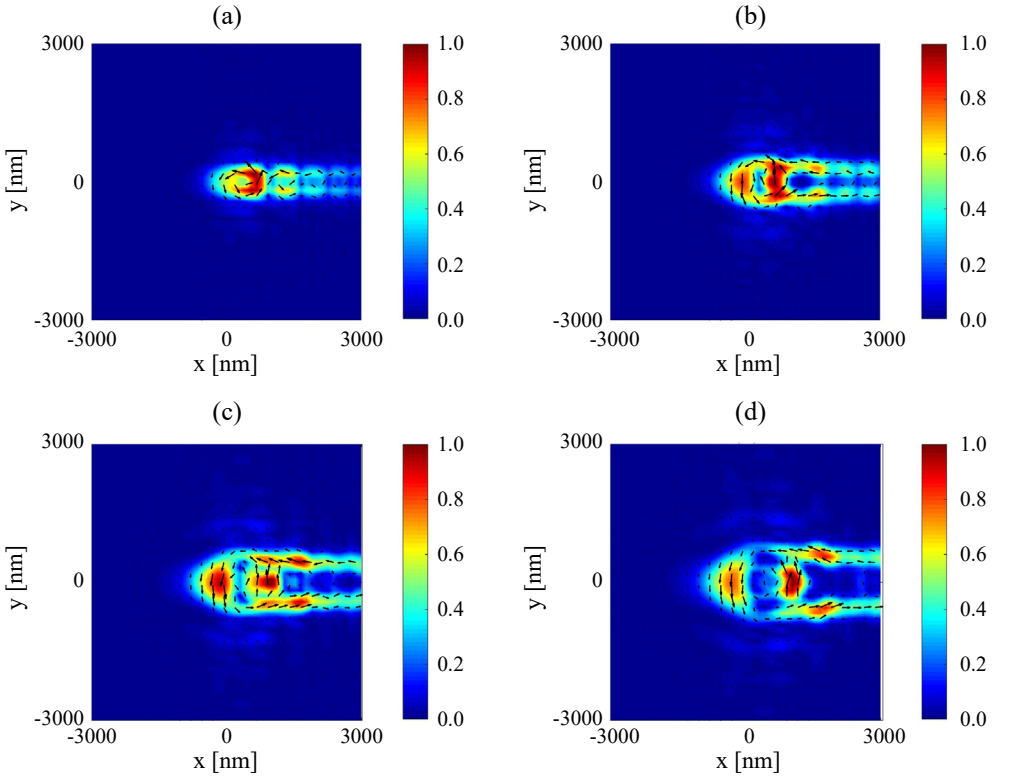

Fig. 5. Normalized transverse (S_{x+y}) energy flow distributions when $n = 3$, $C = 3$ and (a) $m = 1$, (b) $m = 2$, (c) $m = 3$, and (d) $m = 4$. The directional orientation of energy flow is represented by the black arrows.

verse energy flow is distributed like bullets and the energy is mainly concentrated at the head of the bullet, as shown in Fig. 5(a). When $m = 2$, there is a trend of energy diffusion, as shown in Fig. 5(b). When m increases from 3 to 4, there is a tendency for multiple parts of energy to gradually separate while diffusing, as shown in Fig. 5(c) and Fig. 5(d), respectively. This indicates that the energy shows a gradually dispersing trend as m grows. In Fig. 5(a)–(d), the energy flow is in a counterclockwise direction.

Figure 6 shows the transverse energy flow distributions of an azimuthally polarized Lorentz–Gaussian beam when $n = 4$, $C = 3$, and different m. When $m = 1$, the transverse energy is mainly concentrated in two regions and exhibits a reverse Z-shaped distribution, as shown in Fig. 6(a). When $m = 2$, the transverse energy is mainly concentrated in four regions, but the energy density of the regions near the two new focal points is lower than that of the previous two regions, as shown in Fig. 6(b). When m increases from 3 to 4, the energy density of the two regions near the focal point shows a gradually increasing trend, while the energy density of the other two regions shows a gradually decreasing trend, as shown in Fig. 6(c) and (d), respectively. This

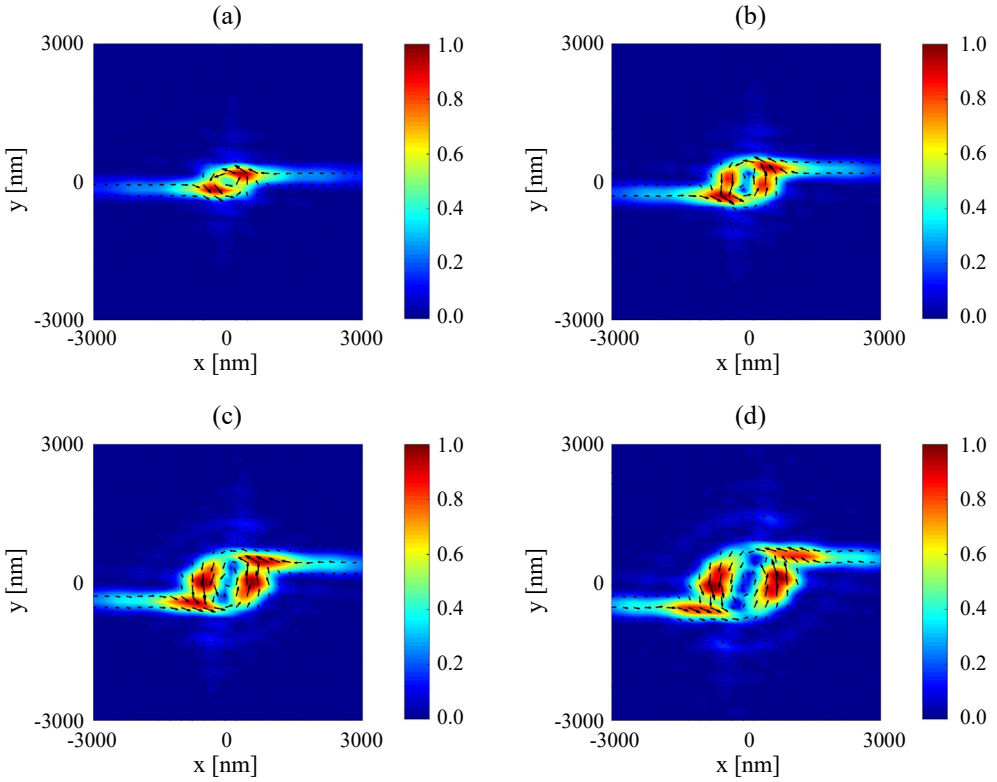

Fig. 6. Normalized transverse (S_{x+y}) energy flow distributions when $n = 4$, $C = 3$ and (a) $m = 1$, (b) $m = 2$, (c) $m = 3$, and (d) $m = 4$. The directional orientation of energy flow is represented by the black arrows.

indicates that energy progressively accumulates in the vicinity of the focal point as m grows. In Fig. 6(a)–(d), the energy flow is in a counterclockwise direction.

4. Conclusions

In the focusing field of an azimuthally polarized Lorentz–Gaussian beam modulated by power order space-variant phase modulation, the transverse energy flow patterns are examined in this study. The research results indicate that when power order phase is not added, the transverse energy flow shows a circular distribution. Additionally, as the topological charge m increases, the energy flow loop's radius progressively grow. When $n = 1$ and $m = 3$, the transverse energy flow still follows a circular distribution. When C is negative, the transverse energy flow ring gradually moves towards the negative x-axis direction as C decreases. While C is a positive number, the transverse energy flow loop gradually moves towards the negative x-axis direction as C decreases. When $n = 2$ and $m = 3$, the transverse energy flow is mainly divided into two parts; When C is negative, the transverse energy in the left half gradually moves towards the

negative x-axis direction as C decreases, while the transverse energy in the right half gradually moves towards the positive x-axis direction as C decreases; When C is a positive number, the transverse energy of the left half gradually moves towards the negative x-axis direction as C increases, while the transverse energy of the right half gradually moves towards the positive x-axis direction as C increases; When $n = 3$ and $C = 3$, the transverse energy flow exhibits a bullet-shaped distribution at $m = 1$, and as m increases, the energy flow gradually spreads; When $n = 4$ and $C = 3$, the transverse energy flow exhibits a reverse Z-shaped distribution, and as m gradually increases, the energy gradually concentrates near the focal point. Additionally, changes in n will have an impact on the overall energy flow distribution. Overall, these unique distributions may contribute to particle capture and transport in different situations.

Acknowledgements
This work was supported by the Ministry of Science and Technology of the People's Republic of China (2021YFF0600204).

References

[1] El. Gawhary O., Severini S., *Lorentz beams and symmetry properties in paraxial optics*, Journal of Optics A: Pure and Applied Optics **8**(5), 2006: 409-414. https://doi.org/10.1088/1464-4258/8/5/007
[2] El. Gawhary O., Severini S., *Lorentz beams as a basis for a new class of rentangularly symmetric optical fields*, Optics Communications **269**(2), 2007: 274-284. https://doi.org/10.1016/j.optcom.2006.08.007
[3] Torre A., Evans W.A.B., El. Gawhary O., Severini S., *Relativistic Hermite polynomials and Lorentz beams*, Journal of Optics A: Pure and Applied Optics **10**(11), 2008: 115007. https://doi.org/10.1088/1464-4258/10/11/115007
[4] Zhou G.Q., *Propagation of a partially coherent Lorentz-Gauss beam through a paraxial ABCD optical system*, Optics Express **18**(5), 2010: 4637-4643. https://doi.org/10.1364/OE.18.004637
[5] Ni Y.Z., Zhou G.Q., *Propagation of a Lorentz–Gauss vortex beam through a paraxial ABCD optical system*, Optics Communications **291**, 2013: 19-25. https://doi.org/10.1016/j.optcom.2012.11.016
[6] Jiang Y.F., Huang K.K., Lu X.H., *Radiation force of highly focused Lorentz-Gauss beams on a Rayleigh particle*, Optics Express **19**(10), 2011: 9708-9713. https://doi.org/10.1364/OE.19.009708
[7] Liu D.J., Wang Y.C., Wang G.Q., Yin H.M., *Influences of oceanic turbulence on Lorentz Gaussian beam*, Optik **154**, 2018: 738-747. https://doi.org/10.1016/j.ijleo.2017.10.113
[8] Sun Q.G., Zhang G.Q., Li C., Yang Y, Gao L., Liu Z.J. Liu, S.T., *Elegant super Lorentz–Gaussian beams*, Optik **126**(7-8), 2015: 774-779. https://doi.org/10.1016/j.ijleo.2015.02.013
[9] Zhang Z.Y., Miao Y, Wang G.X., Sui G.R., Gao X.M., *Focusing properties of radially polarized helico-conical Lorentz-Gauss beam with radial phase wavefront*, Optik **157**, 2018: 93-98. https://doi.org/10.1016/j.ijleo.2017.11.059
[10] Miao Y., Wang G.X., Zhan Q.F., Sui G.R., Zhang R.F., Lu X.M., Gao X.M., *Focal pattern evolution of radially polarized Lorentz-Gaussian vortex beam*, Optik **128**, 2017: 201-206. https://doi.org/10.1016/j.ijleo.2016.10.029
[11] Miao Y., Wang G.X., Shan X.Z., Zeng X.G., Zhang Q.L., Gao X.M., *Focal pattern evolution of azimuthally polarized lorentz-gaussian vortex beam*, Optik **187**, 2019, 17-24. https://doi.org/10.1016/j.ijleo.2019.04.070
[12] Shamsodini N., Honarasa G., *Evolution of four-petal Lorentz–Gauss beams in the strongly nonlocal nonlinear media*, Journal of Nonlinear Optical Physics & Materials **31**(3), 2022: 2250010. https://doi.org/10.1142/S0218863522500102

[13] SUN F., LI Y., WANG G.X., LI Y., DONG X.M., GAO X.M., *Linearly polarized Airy–Lorentz–Gaussian beam modulated by a triangular phase function*, Optik **219**, 2020: 165302. https://doi.org/10.1016/j.ijleo.2020.165302

[14] EBRAHIM A.A.A., YAHYA N.A.A., SWILLAM M.A., BELAFHAL A., *Introduction and propagation properties of circular lorentz-bessel-gaussian beams*, Optical and Quantum Electronics **54**(7), 2022: 434. https://doi.org/10.1007/s11082-022-03868-5

[15] HAWLEY R.D., OFFER R., RADWELL N, FRANKE-ARNOLD S., *Tight focal spots using azimuthally polarised light from a Fresnel cone*, Proceedings of the SPIE, Vol. 11359, Biomedical Spectroscopy, Microscopy, and Imaging, 2020: 1135910. https://doi.org/10.1117/12.2559535

[16] CAO C.Y., LU J.N., ZHANG H.W., ZHU Z.Q., WANG X.L., GU B., *Investigation on magnetization induced by tightly focused azimuthally polarized fractional vortex beam*, Acta Physica Sinica **69**(16), 2020: 167802. https://doi.org/10.7498/aps.69.20200269

[17] MATSUSAKA S., KOZAWA Y., SATO S., *Acceleration of micro-hole drilling by an azimuthally polarized laser beam under tight focusing condition*, 2018 Conference on Lasers and Electro-Optics, 2018. https://doi.org/10.1364/CLEO_SI.2018.SM4O.2

[18] GUAN J., LIN J., CHEN C., MA Y., TAN J.B., JIN P., *Transversely polarized sub-diffraction optical needle with ultra-long depth of focus*, Optics Communications **404**, 2017: 118-123. https://doi.org/10.1016/j.optcom.2017.04.003

[19] SHEN Z., HUANG S., *Generation of subdiffraction optical needles by simultaneously generating and focusing azimuthally polarized vortex beams through Pancharatnam–Berry metalenses*, Nanomaterials **12**(22), 2022: 4074. https://doi.org/10.3390/nano12224074

[20] CHI J., TAO G., *The study of tight focusing characteristics of azimuthally polarized vortex beams and the implementation of ultra-long super-resolved optical needle*, Acta Physica Sinica **72**(12), 2023: 124201. https://doi.org/10.7498/aps.72.20230304

[21] ALKELLY A.A., AL-AHSAB H.T., CHENG M.J., LOQMAN I.G.H., *Tight focusing of azimuthally polarized Laguerre-Gaussian vortex beams by diffractive axicons*, Physica Scripta **99**(2), 2024: 025508. https://doi.org/10.1088/1402-4896/ad1958

[22] YANG Y.F., YAN X.Y., HE Y., DUAN H.H., LI L.L., *Generating and converting special focal field patterns in a 4Pi focusing system illuminated by azimuthally polarized vortex beam*, Optical Review **29**(4), 2022: 320-326. https://doi.org/10.1007/s10043-022-00748-x

[23] DENG D.M., DU S.L., GUO Q., *Energy flow and angular momentum density of nonparaxial Airy beams*, Optics Communications **289**, 2013: 6-9. https://doi.org/10.1016/j.optcom.2012.09.007

[24] GAO X.Z., PAN Y., ZHANG G.L., ZHAO M.D., REN Z.C., TU C.G., LI Y.N., WANG H.T., *Redistributing the energy flow of tightly focused ellipticity-variant vector optical fields*, Photonics Research **5**(6), 2017: 640-648. https://doi.org/10.1364/PRJ.5.000640

[25] JIAO X.Y., LIU S., WANG Q., GAN X.T., LI P., ZHAO J.L., *Redistributing energy flow and polarization of a focused azimuthally polarized beam with rotationally symmetric sector-shaped obstacles*, Optics Letters **37**(6), 2012: 1041-1043. https://doi.org/10.1364/OL.37.001041

[26] MAN Z.S., LI X.Y., ZHANG S.S., BAI Z.D., LYU Y.D., LI J.J., GE X.L., SUN Y.P., FU S.G., *Manipulation of the transverse energy flow of azimuthally polarized beam in tight focusing system*, Optics Communications **431**, 2019: 174-180. https://doi.org/10.1016/j.optcom.2018.09.028

[27] KHONINA S.N., PORFIREV A.P., USTINOV A.V., KIRILENKO M.S., KAZANSKIY N.L., *Tailoring of inverse energy flow profiles with vector Lissajous beams*, Photonics **9**(2), 2022: 121. https://doi.org/10.3390/photonics9020121

[28] CHEN R.X., SONG T.G., LUO Y.E., LI H.H., LI X.Z., *Inverse energy flux in tight focusing of vector vortex beam*, Photonics **10**(7), 2023: 743. https://doi.org/10.3390/photonics10070743

[29] KOTLYAR V.V., KOVALEV A.A., NALIMOV A.G., STAFEEV S.S., TELEGIN A.M., *Transverse and longitudinal energy flows in a sharp focus of vortex and cylindrical vector beams*, Applied Sciences **14**(14), 2024: 6305. https://doi.org/10.3390/app14146305

[30] WOLF E., *Electromagnetic diffraction in optical systems. I. An integral representation of the image field*, Proceedings of the Royal Society of London **253**(1274), 1959: 349-357. https://doi.org/10.1098/rspa.1959.0199

[31] RICHARDS B., WOLF E., *Electromagnetic diffraction in optical systems. II. Structure of the image field in an aplanatic system*, Proceedings of the Royal Society of London **253**(1274), 1959: 358-379. https://doi.org/10.1098/rspa.1959.0200

[32] KOTLYAR V.V., KOVALEV A.A., NALIMOV A.G., *Energy density and energy flux in the focus of an optical vortex: Reverse flux of light energy*, Optics Letters **43**(12), 2018: 2921-2924. https://doi.org/10.1364/OL.43.002921

[33] WANG H., SHI L., LUKYANCHUK B., SHEPPARD C., CHONG C.T., *Creation of a needle of longitudinally polarized light in vacuum using binary optics*, Nature Photonics **2**(8), 2008: 501-505. https://doi.org/10.1038/nphoton.2008.127

Received March 16, 2025
in revised form April 22, 2025